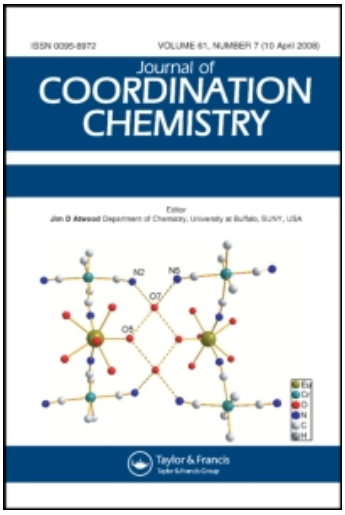

Journal of Coordination Chemistry
Publication details, including instructions for authors and subscription information:
http://www.informaworld.com/smpp/title~content=t713455674

Synthesis, characterization, thermal studies, and antimicrobial activity of 2-(2-(3,4-dihydronaphthalenylidene)hydrazinyl)-2-oxo-N-phenylacetamide (H_2NHPA) and its transition metal complexes

Issam M. Gabr[a]
[a] Chemistry Department, Faculty of Science, Mansoura University, Mansoura, Egypt

To cite this Article Gabr, Issam M.(2009) 'Synthesis, characterization, thermal studies, and antimicrobial activity of 2-(2-(3,4-dihydronaphthalenylidene)hydrazinyl)-2-oxo-N-phenylacetamide (H_2NHPA) and its transition metal complexes', Journal of Coordination Chemistry, 62: 19, 3206 — 3216
To link to this Article: DOI: 10.1080/00958970903019491
URL: http://dx.doi.org/10.1080/00958970903019491

Journal of Coordination Chemistry
Vol. 62, No. 19, 10 October 2009, 3206–3216

Taylor & Francis
Taylor & Francis Group

Synthesis, characterization, thermal studies, and antimicrobial activity of 2-(2-(3,4-dihydronaphthalenylidene)-hydrazinyl)-2-oxo-N-phenylacetamide (H_2NHPA) and its transition metal complexes

ISSAM M. GABR*

Chemistry Department, Faculty of Science, Mansoura University, Mansoura, Egypt

(*Received 20 January 2009; in final form 18 March 2009*)

Complexes of Ni(II), Co(II), Cu(II), Cd(II), Hg(II), and U(VI)O_2 with 2-(2-(3,4-dihydronaphthalenylidene)hydrazinyl)-2-oxo-N-phenylacetamide (H_2NHPA) have been prepared and characterized by elemental analysis, molar conductance, thermal (TG, DTG), spectral (^{1}H NMR, IR, UV–Vis, ESR), and magnetic measurements. IR spectra show that H_2NHPA is a bidentate ligand. Thermal decomposition of some complexes ended with metal oxide as a final product. The room temperature solid state ESR spectra of the Cu(II) complex shows an axial spectrum with $d_{x^2-y^2}$ ground state, suggesting distorted octahedral geometry around Cu(II). Molecular modeling calculations were used to characterize the complex species. The ligand and its complexes were also evaluated against the growth of some bacteria.

Keywords: Hydrazone complexes; ESR; Thermal studies; Molecular modeling; Biological activities

1. Introduction

Hydrazones are ligands having great physiological and biological activities, and have found use as insecticides, anticoagulants, antitumor agents, antioxidants, and plant growth regulators [1]. Their metal complexes have found applications in nonlinear optics, sensors, medicine, etc. [2]; hydrazones incorporating heterocyclic moieties are well known for their metal-binding ability and exhibit interesting coordination with transition metal ions [3, 4]. Hydrazones are also important for their use as plasticizers and stabilizers for polymers [5, 6], polymerization initiators, and antioxidants [7].

In this article, we report the synthesis and characterization of new complexes of 2-(2-(3,4-dihydronaphthalenylidene)hydrazinyl)-2-oxo-N-phenylacetamide (H_2NHPA) (figure 1), which has several coordination sites with Cu(II), Co(II), Ni(II), Cd(II), Hg(II), and U(VI)O_2. Geometries for complexes have been deduced by elemental analyses, molar conductances, magnetic susceptibilities, thermal, IR, electronic, and ESR spectral studies. The biological activities were also examined. In the absence of

*Email: issam_gabr@yahoo.com

ISSN 0095-8972 print/ISSN 1029-0389 online
DOI: 10.1080/00958970903019491

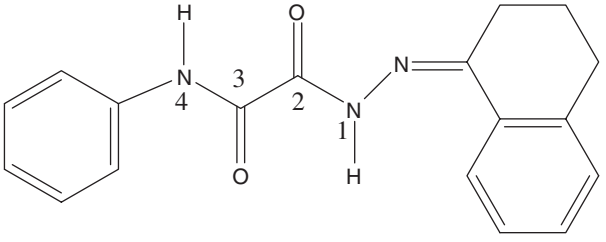

Figure 1. Structure of 2-(2-(3,4-dihydronaphthalenylidene)hydrazinyl)-2-oxo-N-phenylacetamide (H_2NHPA).

suitable crystals for X-ray diffraction, molecular mechanics calculations are performed to give complementary information about probable structures.

2. Experimental

2.1. *Apparatus and reagents*

IR absorption spectra were recorded on a Mattson 5000 FTIR spectrophotometer. Electronic spectra were measured on a Unicam UV-Vis spectrometer UV_2. Thermogravimetric analysis was performed using an automatic recording thermobalance type (951 DuPont instrument). Samples were subjected to heat at the rate of $10^{\circ}C\,min^{-1}$ (25–800°C) in N_2. ^1H NMR spectrum for H_2NHPA, in d_6-DMSO, was recorded on an EM-390 (200 MHz) spectrometer. Carbon and hydrogen content for the ligand and its complexes were determined at the Microanalytical Unit, Mansoura University, Egypt. Ni(II), Co(II), Cu(II), Cd(II), Hg(II), U(VI)O_2, Cl^-, and SO_4^{2-} contents in the complexes were determined by standard methods [8]. ESR spectra were obtained on a Bruker EMX spectrometer working in the X-band (9.78 GHz) with 100 kHz modulation frequency. The microwave power was set at 1 mW and modulation amplitude was set at 4 Gauss. The low field signal was obtained after 4 scans with a 10-fold increase in the receiver gain. A powder spectrum was obtained in a 2 mm quartz capillary at room temperature. All metal salts were pure (Fluka, Aldrich or Merck).

2.2. *Preparation of the ligand*

2-Hydrazino-2-oxo-N-phenyl acetamide was synthesized according to the general literature [9] method by boiling 8 mL of aniline with 8.5 mL of diethyl oxalate; the product was crystallized in water, then 1.65 g of this product was refluxed with 0.5 mL of hydrazine hydrate. H_2NHPA was prepared by boiling an ethanolic solution of 2-hydrazino-2-oxo-N-phenyl acetamide (1.79 g, 0.1 mol) and α-tetralone (1.46 g, 0.1 mol). The isolated compound was filtered off, recrystallized from absolute ethanol, and finally dried in a vacuum desiccator over anhydrous calcium chloride. The purity of the ligand was checked by TLC.

2.3. *Preparation of complexes*

All complexes were prepared by refluxing equimolar amounts of metal chlorides or acetates and the ligand in absolute ethanol for 2–3 h. The resulting solid complexes were

filtered off while the solution was hot, washed with ethanol followed by diethyl ether, dried, and stored in a vacuum desiccator over anhydrous $CaCl_2$.

2.4. *Antimicrobial activity*

The *in vitro* antibacterial activities of the ligand and its complexes were tested against G(+) *Bacillus subtilis* and G(−) *Pseudomonas aeruginosa*. The liquid medium containing the bacterial subcultures was autoclaved for 20 min at 120°C. The bacteria were then cultured for 24 h at 36°C in an incubator. The seeded agar plates were prepared by putting 50 mL of inoculated agar into 15 cm Petri dishes and allowed to solidify. Cups were made to receive 25 µL of the test compounds (DMSO solutions), and allow diffusing and incubating at 37°C for 24 h [10]. The results were compared with gentamicin drug solution (commercial antibiotic, Memphis Co., Egypt, 250 µg mL^{-1}). Three replicas were made for each treatment.

2.5. *Molecular modeling*

All theoretical calculations were performed on a Pentium 4 (3 GHz) computer using HyperChem 7.5 (HyperChem 7.51 Version, Hypercube Inc, Florida, USA, 2003). Initially, molecular geometries of the ligand and its complexes were optimized using molecular mechanics (MM+). Then, low lying states obtained from MM+ were optimized at the Semi-Empirical Parametrization Model 3 (PM3) using the Polak–Ribiere algorithm in RHF-SCF, set to terminate at an RMS gradient of 0.01 kcal Å^{-1} mol^{-1} and convergence limit fixed to 1×10^{-8} kcal mol^{-1}. Afterward, vibrational analysis and electronic spectra were performed by PM3 and RHF-SCF ZINDO/S calculations, respectively.

3. Results and discussion

The elemental analyses showed different stoichiometries for the isolated metal complexes (table 1). The complexes have high melting points (>300°C) and are insoluble in most common solvents but soluble in DMF or DMSO.

3.1. *IR and ^{1}H NMR spectra*

The ^{1}H NMR spectrum of H_2NHPA in d_6-DMSO shows multiplets in the 7.2–8.3 range assigned to aromatic protons. Signals at 11.4 are assigned to (NH) amide protons. The presence of a NH proton in the downfield region may be due to the involvement of this group in hydrogen bonding with d_6-DMSO, which is known to interact with amide proton [11]. The IR spectrum of H_2NHPA shows bands at 1685, 1663, 1604, 3257, and 3294 cm^{-1} assigned to ν(C=O)^2, ν(C=O)^3 [12], ν(C=N) [13], ν(NH)^4, and ν(NH)^3 [14].

Measurements of the pH values of the reaction mixtures for Ni(II), Co(II), and U(VI)O_2 complexes showed a marginal decrease (2.5–3), attributed to the release of H^+ into solution. However, the pH is in the range 4.4–4.8 for Cu(II), Cd(II), and Hg(II) complexes, indicating the ligand is neutral.

Table 1. Analytical and physical data of H_2NHPA and its metal complexes.

Compound	Empirical formula (Formula weight)	Color	pH of the mixture	m.p. (°C)	Yield (%)	% Found (Calcd) C	H	M	X	Λ_m*
H_2NHPA	$C_{18}H_{17}N_3O_2$ (307.35)	Pale yellow	–	244	88	69.81 (70.34)	5.35 (5.58)	–	–	–
$[Cu(H_2NHPA)Cl_2(H_2O)_2]$	$C_{18}H_{21}Cl_2CuN_3O_4$ (477.83)	Olive green	4.8	>300	75	45.36 (45.24)	4.22 (4.43)	14.95 (14.84)	7.85 (7.72)	6
$[UO_2(HNHPA)(OAc)(H_2O)_2]\cdot H_2O$	$C_{20}H_{26}N_3O_9U$ (690.46)	Yellow	2.5	>300	78	34.92 (34.79)	3.98 (3.80)	34.54 (34.47)	–	4
$[Hg(H_2NHPA)Cl_2(H_2O)_2]$	$C_{13}H_{22}O_7CuS_2N_4$ (473.716)	Olive green	4.6	>300	80	35.41 (35.22)	3.48 (3.28)	32.85 (32.68)	20.18 (20.26)	5
$[Cd(H_2NHPA)Cl_2(H_2O)_2]$	$Cd_8H_{20}Cl_2N_3O_4C1$ (525.69)	Yellow	4.4	>300	77	41.35 (41.13)	4.05 (3.83)	21.45 (21.38)	–	5
$[Co(HNHPA)(OAc)(H_2O)_2]\cdot 2H_2O$	$C_{20}H_{27}CoN_3O_8$ (496.38)	Brown	2.7	>300	70	48.66 (48.39)	5.75 (5.48)	12.01 (11.87)		6
$[Ni(HNHPA)(OAc)(H_2O)_2]\cdot 2H_2O$	$C_{20}H_{27}N_3NiO_8$ (496.14)	Yellow	3.0	>300	78	48.65 (48.42)	5.77 (5.49)	12.03 (11.83)		7

*In DMSO ($\Omega^{-1}\,cm^2\,mol^{-1}$).

Comparison of the IR spectrum of the ligand with those of its metal complexes (table 2) reveals that H_2NHPA is bidentate and/or tridentate depending on the metal salt and the reaction conditions.

IR spectra of $[Cu(H_2NHPA)Cl_2(H_2O)_2]$ indicates a neutral bidentate ligand coordinating *via* (C=N) and $(C{=}O)^2$ forming a five-membered ring including the metal. This behavior is supported by a negative shift of both ν(C=N) and $\nu(C{=}O)^2$, while the $\nu(C{=}O)^3$ group remains at the same position. Also, the IR spectra show new bands at 505 and 420 cm^{-1} assignable to ν(Cu–O) and ν(Cu–N) [15].

In $[Hg(H_2NHPA)Cl_2(H_2O)_2]$ and $[Cd(H_2NHPA)Cl_2(H_2O)_2]$, the ligand is neutral bidentate coordinating via two carbonyl oxygens; this mode is supported by the shift of both $\nu(C{=}O)^2$ and $\nu(C{=}O)^3$ to lower wavenumbers while the azomethine and the (NH) groups remain at the same positions. IR spectra of these complexes show new bands in the 503–508, 405–420, and 270–290 cm^{-1} regions assignable to ν(M–O), ν(M–N), and ν(M–Cl) [16], respectively.

In $[Co(HNHPA)(OAc)(H_2O)_2]\cdot 2H_2O$, $[UO_2(HNHPA)(OAc)(H_2O)_2]\cdot H_2O$, and $[Ni(HNHPA)(OAc)(H_2O)_2]\cdot 2H_2O$ (figure 2), the ligand is mononegative bidentate coordinating via the $(C{=}O)^3$ and deprotonated enolized carbonyl group $(=C{-}O^-)^2$.

Table 2. Most important IR spectral bands of H_2NHPA and its metal complexes.

Compound	ν(C=N)	$\nu(C{=}O)^2$	$\nu(C{=}O)^3$	$\nu(NH)^1$	$\nu(NH)^4$	ν(C–O)	ν(M–O)	ν(M–N)	ν(M–Cl)
H_2NHPA	1604	1685	1663	3257	3294	–	–	–	–
$[Cu(H_2NHPA)Cl_2(H_2O)_2]$	1585	1670	1663	3250	3294	–	505	420	296
$[UO_2(HNHPA)(OAc)(H_2O)_2]\cdot H_2O$	1595		1635		3295	1122	510	431	
$[Hg(H_2NHPA)Cl_2(H_2O)_2]$	1603	1669	1649	3260	3290	–	508	405	270
$[Cd(H_2NHPA)Cl_2(H_2O)_2]$	1604	1673	1641	3262	3290	–	503	420	290
$[Co(HNHPA)(OAc)(H_2O)_2]\cdot 2H_2O$	1606	–	1630	–	3295	1127	510	411	–
$[Ni(HNHPA)(OAc)(H_2O)_2]\cdot 2H_2O$	1604	–	1631	–	3295	1118	501	411	–

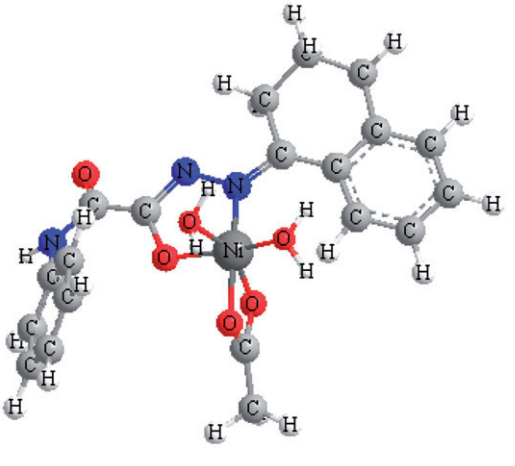

Figure 2. Optimized structure for $[Ni(HNHPA)(OAc)(H_2O)_2]\cdot 2H_2O$.

This mode of complexation is supported by the shift of $\nu(C{=}O)^3$ to lower wavenumber and the disappearance of the $\nu(C{=}O)^2$ with simultaneous appearance of new bands in the 1118–1127 cm^{-1} range assignable to $\nu(C{-}O)_{enolic}$.

Complexes which have coordinated water have two sharp bands at 852–862 and 748–774 cm^{-1} attributed to $\rho_r(H_2O)$ and $\rho_w(H_2O)$ [17], respectively.

The acetate complexes show two bands at 1519–1557 and 1402–1447 cm^{-1}, assigned to $\nu_{as}(O{-}C{-}O)$ and $\nu_s(O{-}C{-}O)$ of acetate. The difference between those two bands indicates bidentate bonding for acetate [18].

The IR spectrum of $[UO_2(HNHPA)(OAc)(H_2O)_2]\cdot H_2O$ displays bands at 943, 760, and 265 cm^{-1}, assigned to ν_3, ν_1, and ν_4 vibrations, respectively, of the dioxouranium ion. The ν_3 value is used to calculate the force constant (F) of $\nu(U{=}O)$ by the method of McGlynn and Smith [19].

$$(\nu_3)^2 = (1307)^2(F_{U-O})/14.103.$$

The force constant obtained for uranyl complex was then substituted into the relation given by Jones [20] to give an estimate of the (U–O) bond length in Å

$$R_{U-O} = 1.08(F_{U-O})^{-\frac{1}{3}} + 1.17.$$

The calculated F_{U-O} and R_{U-O} values of 7.34 mdynes $Å^{-1}$ and 1.72 Å, respectively, fall in the usual range for uranyl complexes.

3.2. *Electronic and magnetic moment measurements*

Magnetic moments and electronic spectral bands in DMF are collected in table 3. The ligand has bands at 32,690 and 28,430 cm^{-1} due to the $\pi \rightarrow \pi^*$ and $n \rightarrow \pi^*$ transitions, respectively [21].

The electronic spectrum of $[Ni(HNHPA)(OAc)(H_2O)_2]\cdot 2H_2O$ (Supplemental Material, figure 3S) shows bands at 15,385 and 25,773 cm^{-1} attributed to $^3A_{2g}(F) \rightarrow {}^3T_{1g}(F)$ and $^3A_{2g}(F) \rightarrow {}^3T_{1g}(P)$ transitions, respectively, indicating that the complex has octahedral geometry and might possess D_{4h} symmetry [22].

The electronic spectrum of $[Co(HNHPA)(OAc)(H_2O)_2]\cdot 2H_2O$ exhibits bands at 17,094 and 20,747 cm^{-1} attributed to $^4T_{1g}(F) \rightarrow {}^4A_{2g}(F)$ and $^4T_{1g}(F) \rightarrow {}^4T_{1g}(P)$ transitions, respectively, in an octahedral configuration [22].

The magnetic moment of $[Cu(H_2NHPA)Cl_2(H_2O)_2]$ at room temperature is 1.88 BM corresponding to one unpaired electron. The complex shows a broad band at 16,650 cm^{-1}

Table 3. Magnetic moments, electronic spectra, and ligand field parameters of metal complexes of H_2NHPA.

Compound	μ_{eff} (BM)	Band position (cm^{-1})	D_q (cm^{-1})	B (cm^{-1})	β	ν_2/ν_1
$[Cu(H_2NHPA)Cl_2(H_2O)_2]$	1.88	14,345; 16,877				
$[UO_2(HNHPA)(OAc)(H_2O)_2]\cdot H_2O$	0.00	23,971; 27,865	–	–	–	–
$[Hg(H_2NHPA)Cl_2(H_2O)_2]$	0.00	14,211; 16,597	–	–	–	–
$[Co(HNHPA)(OAc)(H_2O)_2]\cdot 2H_2O$	5.00	17,094; 20,747	765	923	0.95	2.14
$[Ni(HNHPA)(OAc)(H_2O)_2]\cdot 2H_2O$	3.40	13,605; 24,380	980	700	0.94	1.57
$[Cd(H_2NHPA)Cl_2(H_2O)_2]$	0.00	14,285; 16,393	–	–	–	–

with a shoulder at 1420 cm^{-1} which may be assigned to $^2B_{1g} \rightarrow {}^2E_g$ and $^2E_g \rightarrow {}^2A_{1g}$ transitions, respectively, in a tetragonally distorted octahedral configuration [23].

The electronic spectrum of $[UO_2(HNHPA)(OAc)(H_2O)_2] \cdot H_2O$ shows bands at 23,971 and 27,865 cm^{-1} ascribed to $^1\Sigma_g^+ \rightarrow {}^2\pi_u$ transition for dioxouranium(VI) and charge transfer $n \rightarrow \pi^*$, respectively [24].

3.3. *Ligand field parameters*

Various ligand field parameters calculated for $[Ni(HNHPA)(OAc)(H_2O)_2] \cdot 2H_2O$ and $[Co(HNHPA)(OAc)(H_2O)_2] \cdot 2H_2O$ are listed in table 3. The values of D_q were calculated from transition energy ratio diagram using the ν_3/ν_2 ratio [22]. These results are in agreement with the complexes reported earlier [25]. The nephelauxetic parameter β was readily obtained by using the relation $\beta = B(\text{complex})/B(\text{free ion})$, where B is the Racah inter-electronic repulsion parameter. The lowering in the B value from the free ion values of Ni(II) (1041 cm^{-1}) and Co(II) (971 cm^{-1}) suggests an appreciable covalent character of metal ligand "σ" bond. The calculated values of D_q, B, β, and ν_2/ν_1 for Co(II) and Ni(II) complexes lie in the range reported for an octahedral structure. Also, the magnetic moment values ($\mu_{eff} = 3.40$ and 5.00 BM) for Ni(II) and Co(II) complexes, respectively, are additional evidence for octahedral geometry.

3.4. *Thermal analysis*

In copper complex (Supplemental Material, figure 4S), the initial weight loss of 7.55% (Calcd 7.54%) in the temperature range of 130–231°C (table 4) accounts for loss of two coordinated water molecules. In the second step, weight loss of 14.80% (Calcd 14.80%) in the temperature range of 230–350°C is due to loss of two coordinated chlorides. The complex then decomposes into two steps leaving behind CuO at 718°C with residue of 16.66%, which agrees with metal analysis.

The TG curve of $[Ni(HNHPA)(OAc)(H_2O)_2] \cdot 2H_2O$ (Supplemental Material, figure 5S) displays weight loss of 7.28% (Calcd 7.25%) in the 36–120°C temperature range due to loss of two water molecules. In the temperature range 120–185°C, the TG curve displays 7.26%

Table 4. Thermal behavior of $[Cu(H_2NHPA)Cl_2(H_2O)_2]$ and $[Ni(HNHPA)(OAc)(H_2O)_2] \cdot 2H_2O$ complexes.

			Wt. loss %	
Complex (Mol. wt)	Temp. range (°C)	Decomposition products (Formula wt)	Found	Calcd
$[Cu(H_2NHPA)Cl_2(H_2O)_2]$ (477.829)	130–231	$2H_2O$ (36.032)	7.55	7.54
	331–400	Cl_2 (70.905)	14.80	14.80
	468–622	$C_{10}H_{10}N$ (144.19)	30.26	30.20
	622–718	$C_8H_7N_2O$ (147.15)	30.90	30.80
	>718	CuO (79.54)	16.70	16.66
$Ni(HNHPA)(OAc)(H_2O)_2] \cdot 2H_2O$ (496.14)	36–120	$2H_2O$ (36.032)	7.28	7.25
	120–185	$2H_2O$ (36.032)	7.26	7.25
	185–308	$C_2H_3O_2$ (59.044)	11.92	11.90
	310–550	$C_{18}H_{17}N_3O$ (291.35)	58.59	58.60
	>550	NiO (74.693)	15.10	15.00

(Calcd 7.25%) weight loss correlated with the release of two coordinated water molecules [26]. In the temperature range 185–308°C, the TG curve displays 11.92% weight loss corresponding to the release of acetate [27]. Further weight loss of 58.59% (Calcd 58.60%) in the temperature range of 310–550°C is assigned to the loss of ligand, leaving NiO comprising 15.1% of the initial weight of the complex.

3.5. *ESR studies*

The room temperature X-band ESR spectrum of powdered $[Cu(H_2NHPA)Cl_2(H_2O)_2]$ (Supplemental Material, figure 6S) was recorded and its spin Hamiltonian parameters were calculated. The ESR spectrum of this complex exhibits axially symmetric g-tensor parameters with $g_{\parallel}$ (2.25) > $g_{\perp}$ (2.06) > 2.0023 indicating that the unpaired electron most likely resides in $d_{x^2-y^2}$ ground state [28]. In axial symmetry, the g-values are related by the expression $G = (g_{\parallel} - 2)/(g_{\perp} - 2) = 4$, where G is the exchange interaction parameter. According to Hathaway and Billing [29], if the value of G is greater than 4, then the exchange interaction between Cu(II) centers in the solid state is negligible; whereas when less than 4, considerable exchange interaction is indicated. The calculated G-value (4.2) suggests no copper–copper exchange interaction. The $g_{\parallel}$ is a moderate measure for covalency [29], where $g_{\parallel} > 2.3$ and < 2.3 is characteristic for ionic and covalent metal–ligand bonding. The observed $g_{\parallel}$ value less than 2.3 indicates considerable covalency. The ESR spectrum of copper complex shows the allowed transitions $\Delta M_s = \pm 1$ and has four weakly defined hyperfine lines in the parallel region corresponding to the electron–nuclear spin interaction (^{63}Cu, $I = 3/2$). The fourth copper hyperfine line is expected to overlap with the high field component ($g_{\perp}$). No band corresponding to the forbidden magnetic dipolar transition for the complexes is observed at half-field (*ca* 1500 G, $g = 4.0$), ruling out any Cu–Cu interaction and indicating that the complex is mononuclear [30]. Superhyperfine structure is not seen at high field excluding interaction of the nuclear spin of nitrogen ($I = 1$) with the unpaired electron density of Cu(II).

The tendency of $A_{\parallel}$ (160 cm^{-1}) to decrease with increase of $g_{\parallel}$ is a measure of tetrahedral distortion in the coordination sphere of Cu(II) [31]. In order to quantify the degree of distortion of the Cu(II) complex, f factor, $g_{\parallel}/A_{\parallel}$, is selected from the ESR spectrum. Its value ranges between 105 and 135 for square planar complexes, depending on the nature of the coordinated atoms. In the presence of a tetrahedrally distorted structure, the values are much larger. For this complex, the $g_{\parallel}/A_{\parallel} = 140$ indicates a dihedral angle distortion in the xy-plane, consistent with distorted octahedral geometry around the copper site.

Molecular orbital coefficients, α^2 (a measure of the covalency of the in-plane σ-bonding between a copper 3d orbital and the ligand orbitals) and β^2 (covalent in-plane π-bonding), were calculated by using the following equations, where $\alpha^2 = 1$ indicates complete ionic character and $\alpha^2 = 0.5$ denotes 100% covalent bonding, with assumption of negligibly small values of the overlap integral [29, 32–35].

$$\alpha^2 = (A_{\parallel}/0.036) + (g_{\parallel} - 2.0023) + 3(g_{\perp} - 2.0023)/7 + 0.04,$$

$$\beta^2 = (g_{\parallel} - 2.0023)E/ - 8\lambda\alpha^2,$$

where $\lambda = -828\,cm^{-1}$ for free copper ion and E is the electronic transition energy. The lower value of $\beta^2(0.71)$ compared to $\alpha^2(0.75)$ indicates that the in-plane σ-bonding is less covalent than the in-plane π-bonding. The α^2 value for copper(II) complex indicates considerable covalency in the bonding between the Cu(II) and the ligand.

The calculated values supported the argument that the in-plane σ-bonding and in-plane and out-of-plane π-bonding are appreciably covalent. The data are in agreement with other reported values [36–39].

The room temperature ESR spectrum of Co(II) complex was recorded as polycrystalline sample. No ESR signal was observed at room temperature because the rapid spin lattice relaxation of Co(II) broadens the lines at higher temperature.

3.6. *Antibacterial activity*

Results of antibacterial screening against *B. subtilis* and *P. aeruginosa*, summarized in table 5, indicate that the metal complexes have higher antibacterial activity than the control. The antimicrobial data reveal that the complexes are more bioactive than the free ligand. The enhanced activity of the metal complexes may be ascribed to the increased lipophilic nature of these complexes arising due to chelation. Growth inhibition zones are proportional to the antimicrobial activity of the tested compounds. The data suggest that Gram-positive and Gram-negative bacteria were affected by the tested chemicals. Co(II) and Hg(II) are the most potent in killing *B. subtilis* and *P. aeruginosa*.

3.7. *Molecular modeling*

The corresponding structures generated by (MM+) molecular simulation for the ligand and its complexes, taking Ni(II) complex as a representative example (figure 2), exhibit strong distortions from planar. Molecular modeling simulations show that the complexes have octahedral structure around the metal. The simulation of IR and UV–Vis spectra by semiempirical PM3 method shows agreement with experimental data. The energy demands on conformational rearrangement are considered reasonable in view of the flexible nature of the ligand system. Other structures were also

Table 5. Inhibited zones diameter (I.Z.D.) in mm as a criterion of antibacterial activity of the ligand and its complexes at concentration level of 2 mg L^{-1}.

	Bacteria	
	B. subtilis (G+ve)	*P. aeruginosa* (G–ve)
Gentamicin	20.7 ± 0.2	23.6 ± 0.2
H_2NHPA	15.0 ± 0.2	16.0 ± 0.2
$[Cu(H_2NHPA)Cl_2(H_2O)_2]$	27.0 ± 0.1	22.0 ± 0.1
$[UO_2(HNHPA)(OAc)(H_2O)_2]\cdot H_2O$	24.0 ± 0.2	25.0 ± 0.2
$[Hg(H_2NHPA)Cl_2(H_2O)_2]$	31.0 ± 0.2	28.0 ± 0.2
$[Co(HNHPA)(OAc)(H_2O)_2]\cdot 2H_2O$	33.0 ± 0.2	29.0 ± 0.2
$[Ni(HNHPA)(OAc)(H_2O)_2]\cdot 2H_2O$	18.0 ± 0.1	14.0 ± 0.2
$[Cd(H_2NHPA)Cl_2(H_2O)_2]$	22.0 ± 0.2	17.0 ± 0.1

Values are mean ± SEM of three replicate experiments.

investigated by molecular modeling and were found to have higher strain energy than the structure presented, and were therefore discarded.

4. Conclusion

A new hydrazone ligand and its Ni(II), Co(II), Cu(II), Cd(II), Hg(II), and U(VI)O_2 complexes have been synthesized and characterized by elemental analyses, spectral, magnetic, conductance measurements, thermal, and theoretical methods. H_2NHPA is a bidentate ligand forming mononuclear complexes. All the measurements confirmed distorted octahedral geometry around the metal. The ESR analysis of the Cu(II) complex revealed appreciable covalency in the metal–ligand bonding. The thermal decomposition of Ni(II) and Cu(II) complexes is discussed in relation to structure and different thermodynamic parameters of some decomposition stages are evaluated. The ligand and its metal complexes exhibit antimicrobial activity against *B. subtilis* and *P. aeruginosa*.

References

[1] Y.P. Kitaev, B.I. Buzykin, T.V. Troepolskaya. *Russ. Chem. Rev.*, **39**, 441 (1970).
[2] M. Bakir, I. Hassan, T. Johnson, O. Brown, O. Green, C. Gyles, M.D. Coley. *J. Mol. Struct.*, **688**, 213 (2004).
[3] A.E. Dissouky, O.A. Fulij, S.S. Kandil. *J. Coord. Chem.*, **57**, 605 (2004).
[4] N. Nawar, N.M. Hosny. *Chem. Pharm. Bull.*, **47**, 944 (1999).
[5] U. Kuehn, S. Warzeska, H. Pritzkow, R. Kraemer. *J. Am. Chem. Soc.*, **123**, 6125 (2001).
[6] K.D. Karlin, J. Zubieta. *Copper Coordination Chemistry: Biochemistry Chemical and Inorganic Perspectives*, Adenine Press Guilderland, New York (1983).
[7] A.G. Mauk, R.A. Scott, H.B. Gray. *J. Am. Chem. Soc.*, **102**, 4360 (1980).
[8] A.I. Vogel. *Quantitative Inorganic Analysis*, Longmans, London (1989).
[9] L.A. Cescon, A.R. Day. *J. Org. Chem.*, **27**, 581 (1962).
[10] P. Gerhardt. *Manual of Methods for General Bacteriology*, American Society for Microbiology, Castello (1981).
[11] L.A. La Planche, M.T. Rogers. *J. Am. Chem. Soc.*, **86**, 337 (1964).
[12] M.M. Mostafa, M.A. Khattab, K.M. Ibrahim. *Polyhedron*, **2**, 583 (1983).
[13] F.B. Tamboura, P.M. Haba, M. Gaye, A.S. Sall, A.H. Barry, T. Jouini. *Polyhedron*, **23**, 1191 (2004).
[14] R. Gup, B. Kirkan. *Spectrochim. Acta A*, **62**, 1188 (2005).
[15] D.X. West, D.L. Huffman. *Transition Met. Chem.*, **14**, 190 (1989).
[16] P.N. Yadav, M.A. Demertzis, D. Kovala-Demertzi, S. Skoulika, D.X. West. *Inorg. Chem. Acta*, **349**, 30 (2003).
[17] K. Nakamoto. *Infrared Spectrum of Inorganic and Coordination Compounds*, Wiley, New York (1970).
[18] K.M. Ibrahim, M.M. Bekheit. *Transition Met. Chem.*, **13**, 230 (1988).
[19] S.P. McGlynn, J.K. Smith. *J. Chem. Phys.*, **35**, 105 (1961).
[20] H. Jones. *Spectrochim. Acta A*, **10**, 395 (1958).
[21] F.H. Allen, O. Kennard, D.G. Watson, L. Brammer, A.G. Orpen, R. Taylor. *J. Chem. Soc., Perkin Trans.*, **2**, 1 (1987).
[22] A.B.P. Lever. *Crystal Field Spectrum, Inorganic Electronic Spectroscopy*, 1st Edn, p. 249, Elsevier, Amsterdam (1968).
[23] L. Sacconi. *Transition Met. Chem.*, **4**, 199 (1979).
[24] R.G. Bhattacharya, D.C. Bera. *J. Ind. Chem. Soc.*, **52**, 373 (1975).
[25] N.M. El-Metwally, I.M. Gabr, A.M. Shallaby, A.A. El-Asmy. *J. Coord. Chem.*, **58**, 1154 (2005).
[26] T.H. Rakha, K.M. Ibrahim, M.E. Khalifa. *Thermochim. Acta*, **144**, 53 (1989).
[27] T.H. Rakha, M.M. Bekheit, M.M. El-Agez. *Synth. React. Inorg. Met.-Org. Chem.*, **29**, 449 (1999).
[28] A. Bernalte-Garcia, A.M. Lozano-Vila, F. Luna-Giles, R. Pedrero-Marin. *Polyhedron*, **25**, 1399 (2006).

[29] (a) B.J. Hathaway, D.E. Billing. *Coord. Chem. Rev.*, **5**, 143 (1970); (b) B.J. Hathaway. *Struct. Bonding* (Berlin), **57**, 55 (1984).
[30] S. Youngme, J. Phatchimkun, U. Suksangpanya, C. Pakawatchai, G.A. van Albada, J. Reedijk. *Inorg. Chem. Commun.*, **8**, 882 (2005).
[31] U. Sagakuchi, A.W. Addison. *J. Chem. Soc., Dalton Trans.*, 660 (1979).
[32] R.K. Ray, G.R. Kauffman. *Inorg. Chim. Acta*, **173**, 207 (1990).
[33] E.I. Solomon, M.J. Baldwin, M.D. Lowery. *Chem. Rev.*, **92**, 521 (1992).
[34] K. Jayasubramanian, S.A. Samath, S. Thambidurai, R. Murugesan, S.K. Ramalingam. *Transition Met. Chem.*, **20**, 76 (1995).
[35] V.S.X. Anthonisamy, R. Murugesan. *Chem. Phys. Lett.*, **287**, 353 (1998).
[36] G.A.A. Al-Hazmi, M.S. El-Shahawi, I.M. Gabr, A.A. El-Asmy. *J. Coord. Chem.*, **58**, 713 (2005).
[37] N.M. El-Metwally, I.M. Gabr, A.A. Abou-Hussen, A.A. El-Asmy. *Transition Met. Chem.*, **31**, 71 (2006).
[38] U. El-Ayaan, I.M. Gabr. *Spectrochim. Acta A*, **67**, 263 (2007).
[39] L.D.S. Yadav, S. Singh. *Indian J. Chem., Sect. B*, **40**, 440 (2001).